# Energy Balance Analysis of Nonlinear Combustion Instability

G. A. Flandro*
*University of Utah, Salt Lake City, Utah*

**To be of practical value, analytical models for nonlinear rocket motor combustion instability must adequately represent: 1) steep fronted waves, 2) limit cycle operation, and 3) triggering phenomena. Inclusion of all these effects in an approximate analysis based on perturbation expansion procedures requires retention of terms to at least the third order in the perturbation parameter representing the system amplitude. In this paper, the acoustic energy balance method is extended into the nonlinear regime and combined with a simplified geometrical representation of the wave structure to greatly simplify this procedure. A practical approximate model for axial pressure fluctuations in a tubular rocket motor results. Effects of nonlinear combustion and nonisentropic energy losses in the steep wave fronts are represented. Since the relative amplitudes of the Fourier components that comprise the traveling shock waves may be assumed to remain effectively fixed near amplitude limiting conditions, great mathematical simplifications accrue. The behavior of the system is governed by a simple polynomial expression which gives the rate of change of the composite system amplitude. The coefficients are integral expressions taken over the chamber volume and its bounding surfaces. The familiar exponential growth rate model appears as the first-order (linear) limiting case. The model demonstrates all of the nonlinear characteristics observed in motor data and shows promise as an easily used diagnostic tool. It has been successfully employed to simulate actual experimental results from pulser tests in inert chambers and from sonic end-vent burner tests.**

## Nomenclature

$a_0$ = speed of sound
$A$ = system linear growth rate integral
$B$ = second-order growth rate integral function
$C$ = third-order growth rate integral function
$C_n$ = relative amplitude of mode $n$
$E_n$ = acoustic energy density contribution of order $n$
$F$ = Blokhintsev/Cantrell/Hart energy density correction
$H$ = enthalpy function
$I$ = integrals defined in text
$I_n$ = acoustic intensity vector function of order $n$
$J$ = nozzle throat-to-part area ratio
$k_n$ = wave number
$L$ = chamber length
$L_g$ = propellant grain sample length
$\boldsymbol{m}$ = mass flow rate vector
$M_b$ = Mach number at burning surface
$n$ = mode integer
$\boldsymbol{n}$ = unit vector normal to surface (positive outward)
$p$ = pressure
$P_0$ = mean chamber pressure
$R_b$ = propellant combustion response function
$s$ = entropy
$S$ = surface area
$S_b$ = burning surface area
$S_c$ = chamber cross-sectional area
$\boldsymbol{u}$ = velocity vector
$\boldsymbol{U}_0$ = mean flow velocity vector
$v$ = normal velocity component at burning surface
$\alpha$ = exponential growth rate (equivalent to $A$)
$\gamma$ = ratio of specific heats
$\epsilon$ = amplitude parameter
$\mathrm{E}$ = acoustic energy (volume integral of energy density $E$)
$\xi$ = waveform function $\Sigma C_n^2/4$
$\rho$ = density
$\phi$ = phase angle
$\omega$ = frequency
$\langle\ \rangle$ = time average of enclosed function

*Subscripts*

$0$ = mean reference value
$b$ = value at burning surface
$i$ = imaginary part
$r$ = real part

*Superscripts*

$(\ )^*$ = complex conjugate
$(\ )'$ = time-dependent quantities

Received Oct. 1, 1984; revision received Feb. 16, 1985. 

*Director, Fluid Dynamics Laboratory and Chairman, Division of Fluid Mechanics. Associate Fellow AIAA.

## Introduction

ANALYSES based on aysmptotic perturbation expansions have been used for many years as the basis for nonlinear combustion instability theory.[1] More recently, numerical techniques have been developed that show much promise in yielding quantitative information regarding the possibility for combustion-driven oscillations in a given solid rocket motor design.[2-4] The model presented herein was devised as part of a recent in-depth study of the nonlinear oscillatory behavior of tactical rockets.[5] It is intended to bridge the gap between complete numerical analyses which attempt to trace all details of the system behavior and various simplified conceptual models. The former may require extensive numerical evaluation, which renders them difficult to use in a preliminary design environment wherein one seeks to understand the parametric tradeoffs in a semiquantitative fashion. The motor designer frequently needs to estimate the sensitivity of various nonlinear phenomena to basic system parameters such as motor volume, burning surface area and placement of propellant surfaces, operating pressures, and nozzle configuration. To be useful, any analysis intended to provide this type of design information must address several fundamental attributes of nonlinear time-dependent motor system behavior, including: 1) steep wave fronts, 2) limit cy-

cle operation, and 3) triggering phenomena. To incorporate all such attributes in a truly general way results in an exceedingly complex problem. In this paper, two major assumptions are utilized to minimize these difficulties while still retaining sufficient generality to produce a useful approximate design tool. The main goal of the analysis is to estimate the limiting amplitude if the system is linearly unstable or the lowest triggering amplitude if the system is linearly stable. The model does not attempt to trace the details of the wave steepening process but focuses instead on the behavior of the system after a definite waveform has been established. Experimental data indicate that the spectral content of the wave is often fixed for many cycles of oscillation. Such periods are most often observed as the system approaches the limiting amplitude, during growth after the initial steepening occurs, or during the initial stages of decay. It is useful to assume that the relative amplitudes and phases of the spectral components of the wave system change slowly on a time scale based on the fundamental oscillation period. This allows nonisentropic losses to be accounted for in a straightforward fashion and also allows study of other nonlinear gain/loss mechanisms. The frozen waveform representation is chosen by the analyst on the basis of experience with the particular system geometry, propellant, and grain configuration. It is readily demonstrated that the predicted limit cycle amplitudes are not overly sensitive to changes in the spectral content of the wave.

Some aspects of the nonlinear gasdynamics are represented; the nonlinear shock losses appear to be the dominant contribution to limit cycle operation in finite amplitude longitudinal mode combustion instability in minimum smoke motors. Other mechanisms, such as nonlinear particle damping, may dominate in motors utilizing highly metalized propellants. In the latter case, the damping may preclude steepening; that is, the high-frequency components may be heavily damped and the composite waveform will not exhibit steep fronts. This and similar nonlinear damping mechanisms probably account for most cases involving finite amplitude limit cycle oscillations with nearly sinusoidal waveforms. The approach introduced in this paper can be utilized in any of these situations; however, not all potentially important nonlinear damping mechanisms have been elucidated in sufficient detail to warrant inclusion at the present stage of development.

The triggerability of a motor system is also an important practical concern. This attribute of nonlinear behavior is defined herein in terms of a critical triggering amplitude. If the chamber is pulsed, either deliberately or by random disturbances, in such a way that this critical composite wave amplitude is exceeded, then the oscillations grow to a new limit cycle amplitude. Linearly stable systems may be forced into a finite-limit cycle oscillation at an amplitude higher than the triggering level; linearly unstable systems which have spontaneously grown to the lowest possible limit amplitude may be forced to an even higher amplitude if pulsed above the triggering level. It is necessary to carry out the perturbation series solutions at least to third order in the system amplitude parameter to represent true triggering effects properly. Unfortunately there is not uniform agreement among investigators as to what constitutes triggered behavior. One important application of the anaytical model presented here is in the clarification of this issue. An unambiguous definition of triggering is introduced.

The utility of the proposed method of analysis is demonstrated by its application to several experimental situations. Most of the numerical results presented reflect the geometry and physical parameters represented by a recent comprehensive experimental study of nonlinear combustion instability.[5] A typical burner configuration used in these tests is shown schematically in Fig. 1. The results allow an assessment of the practicability of analytical methods in the modeling of nonlinear oscillatory behavior. Several inherent limitations of the perturbation approach to the modeling problem appear; it is shown that retention of at least third-order terms is necessary if system amplitudes greater than about one-tenth the chamber mean pressure are to be addressed.

## Representation of Steep Fronted Waves

The connection between the shock-like waveform that often characterize nonlinear combustion oscillations and the acoustics of the chamber must be clearly understood. The steep wave fronts can be initiated by pulsing the system, or they can grow from initially weak acoustic disturbances. Examination of the spectral content in typical data of the latter type suggests that steepening comes about as a result of the increasing amplitude and phase shifting of the higher-order acoustic harmonics. This implies that the final traveling shock configuration can be conveniently represented as a superposition of standing acoustic eigenfunctions. For one-dimensional problems, the pressure and velocity are given by

$$\frac{p'}{P_0} = \epsilon \sum_{n=1}^{\infty} C_n \cos(k_n x) \sin(\omega_n t - \phi_n) \tag{1}$$

$$\frac{u'}{a_0} = \epsilon \sum_{n=1}^{\infty} C_n \sin(k_n x) \cos(\omega_n t - \phi_n) \tag{2}$$

where $C_n$ is the relative amplitude of mode $n$ and $\phi_n$ is the relative phase angle. $k_n$ and $\omega_n$ are the wave number and frequency for mode $n$ as given for a tubular chamber of length $L$ by

$$k_n = n\pi/L \quad \text{and} \quad \omega_n = n\pi a_0/L \tag{3}$$

A solution that represents traveling waves in a hard-walled chamber with closed ends is

$$C_n = 8n/\pi(4n^2-1), \qquad \phi_n = 0 \tag{4}$$

This solution exhibits the classical $N$-wave traveling shock pressure distribution; it has the advantage of simplicity since the phase angles are all zero. A solution that better represents the actual waveforms observed in tactical rockets is

$$C_n = 2\sqrt{1+(n\pi)^2}/(n\pi)^2, \qquad \phi_n = -\tan^{-1}[1/(n\pi)] \tag{5}$$

Figure 2 compares the waveform based on this model with pressure fluctuations measured in a sonic end-vent burner.[5] The data and the simulated gas motions represent fluctuations at the chamber head end. Only six terms were retained in the Fourier representation.

Other wave-front geometries are readily constructed; proper choice of the amplitude and phase functions allows realistic analytic representation of any observed waveform. It must be emphasized that the motion described by Eqs. (1) and (2) properly represents in every sense the shock-like behavior in actual systems when a single shock front is present. It is well known that Fourier spectral analysis of motor data is the only practical approach. Unfortunately it has taken some time for

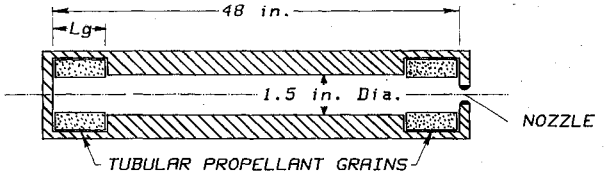


**Fig. 1 Typical sonic and end-vent burner configuration.**

investigators to realize that the Fourier components can be interpreted as standing acoustic waves even though the composite wave motion is observed to be a traveling steep fronted wave.

The parameter $\epsilon$ in Eqs. (1) and (2) represents the composite amplitude of the wave system. Since simulation of the approach to limit cycle or triggering behavior is the aim of the analysis, it is necessary to regard $\epsilon$ as a "slow" function of time. That is, changes in wave amplitude must be represented on a time scale longer than the period of oscillation of the fundamental Fourier component. There are certainly situations where this assumption would not be appropriate; nevertheless, changes in amplitude obviously take place rather slowly as the limit cycle is approached, and it is this situation that is of central interest here. The methods of singular perturbation theory are employed to account for the two time scales inherent in the problem. In fact, there are at least three time scales that govern the motion in a solid propellant system: 1) the period of the fundamental mode of oscillation, 2) the time constant representing changes in system amplitude, and 3) the time scale representative of changes in geometry due to propellant combustion and associated changes in mean properties of the gas flow. Changes of the third type are not represented in the analysis; however, there is evidence that they may be important in interpretation of experimental data. For instance, changes in system amplitude brought about by slowly changing (compared to the oscillations) geometry can be misinterpreted as triggering or evidence of unusual driving or damping mechanisms.

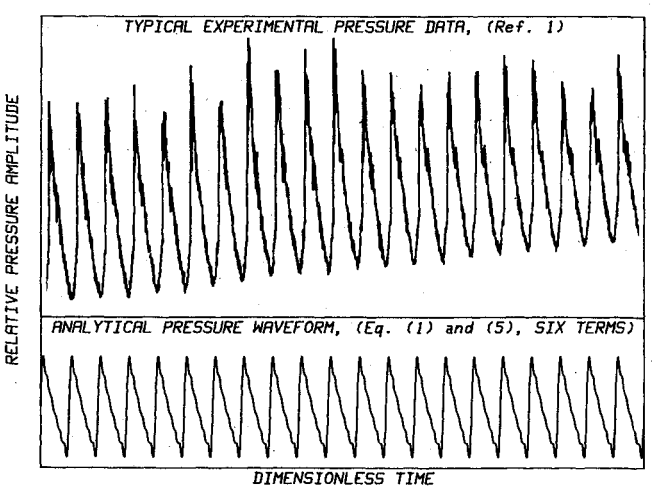


**Fig. 2 Experimental and analytical pressure oscillation waveform.**

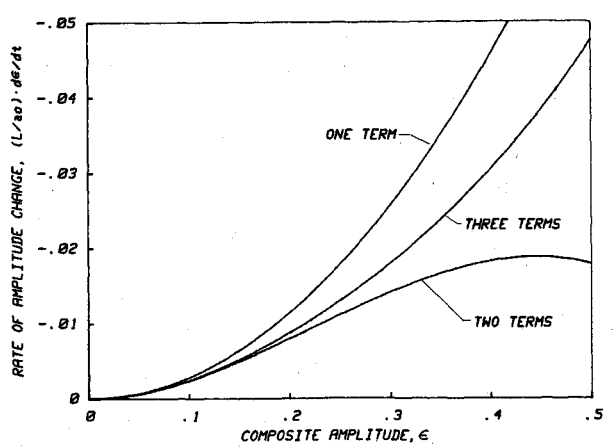


**Fig. 3 Effect of number of terms retained and shock-loss series expansion.**

The acoustic energy contained at a given time within the composite wave structure provides a powerful tool for describing the system behavior. Since this energy clearly depends on the instantaneous value of the system amplitude $\epsilon$, then modeling of the nonlinear system energy gains and losses yields information on the time behavior of the global amplitude.

## Acoustic Energy Balance

If the assumption is made that the waveform changes are negligible during the approach to limiting conditions, then energy transfer between the modes can be ignored. The amplitude at any instant is the result of the balance between the linear and nonlinear losses and gains of system energy. Techniques required for nonlinear energy balance calculations have not been extensively developed for use in rocket stability analysis. Early work in combusiton instability focused on this approach as originally formulated by Cantrell and Hart.[6] Work by Morfey[7] was aimed at clarifying the acoustic energy concept and extending it to problems involving nonlinear acoustic wave generation and propagation in a moving medium. This was based on earlier studies of this problem by Andreev,[8] Markham,[9,10] Blokhintsev,[11] and Schoch.[12] It has proved difficult to define an acceptable nonlinear representation of acoustic energy in a moving medium. Culick[13] questions corrections to the classical linear acoustic energy density introduced by Cantrell and Hart on the basis that they are an order higher than terms eventually retained in the linear analysis of combusition instability. The situation changes when one sets out to assess the nonlinear effects; retention of higher-order terms in the energy density is obviously required. Despite the lack of uniform agreement on what constitutes the correct nonlinear representation, the inherent simplicity and clarity associated with energy balance formulations are so desirable in the present context that a fresh look at this approach to the problem seems appropriate. What is required is a generalized form of the classical acoustic energy model which states that the rate of change of energy density $E$ is governed by a relationship of the form

$$\frac{dE}{dt} = -\nabla \cdot \boldsymbol{I} + \tilde{P} \tag{6}$$

where $\boldsymbol{I}$ is the acoustic intensity and $\tilde{P}$ represents production of acoustic energy per unit volume. Morfey[7] constructed an expression of this form for wave motions superimposed on a mean flow to second-order (in wave amplitude) accuracy. Unfortunately his formulation employed generalized thermodynamic variables, and no detailed applications to the rocket motor problem were carried out; thus, this fine analysis has been neglected for two decades. It is useful to carefully assess Morfey's approach with the aim of extending it to the required third-order accuracy and putting it in more familiar mathematical form for use in nonlinear instability calculations. The assumption of isentropic flow with no vortical or combustion energy sources within the chamber volume leads to a straightforward formulation for nonlinear gas oscillations. Losses due to shock effects are readily incorporated since they arise in discontinuities; combustion effects are introduced in the form of boundary conditions at burning propellant surfaces as in the conventional linear analysis. If the gas is also assumed to be calorically perfect, the governing continuity and momentum equations can be written as

$$\frac{\partial P}{\partial t} = -\nabla \cdot \boldsymbol{m} \tag{7}$$

$$\frac{\partial u}{\partial t} = -\nabla H \tag{8}$$

where $\boldsymbol{m}$ is the mass flux per unit volume ($\boldsymbol{m}=\rho\boldsymbol{u}$) and $H$ is the enthalpy function, which is defined by

$$\nabla H=\nabla P/\rho+\boldsymbol{u}\cdot\nabla\boldsymbol{u} \tag{9}$$

The energy equation itself collapses to the isentropic relationship between the thermodynamic variables. All variables are comprised of slowly varying and rapidly oscillating components:

$$p=P_0+p', \qquad \rho=\rho_0+\rho', \qquad \boldsymbol{u}=\boldsymbol{U}_0+\boldsymbol{u}' \tag{10}$$

The rapidly oscillating components are taken to be composed of periodic functions represented by the fast time scale and amplitude functions which change slowly as compared to the period of the fluctuations. Equations (10) are used to expand the differential equations and the isentropic relationship for density in terms of the pressure. It is conventient to utilize $\epsilon$, the composite wave amplitude, as a perturbation parameter. The expansions for the primary variables are

$$\begin{aligned}
H' &= \epsilon H_1+\epsilon^2 H_2+\epsilon^3 H_3+\mathcal{O}(\epsilon^4)\\
\boldsymbol{m}' &= \epsilon\boldsymbol{m}_1+\epsilon^2\boldsymbol{m}_2+\epsilon^3\boldsymbol{m}_3+\mathcal{O}(\epsilon^4)\\
\rho' &= \epsilon\frac{p'}{a_0^2}+\epsilon^2\rho_0\frac{(1-\gamma)}{2\gamma^2}\left(\frac{p'}{P_0}\right)^2\\
&\quad+\epsilon^3\rho_0\frac{(1-\gamma)(1-2\gamma)}{6\gamma^3}\left(\frac{p'}{P_0}\right)^3+\mathcal{O}(\epsilon^4)
\end{aligned} \tag{11}$$

where the primes denote the fluctuating, or "acoustic," part of the variable.

Expansion of the enthalpy function yields

$$\begin{aligned}
H_1 &= \frac{p'}{\rho_0}+\boldsymbol{U}_0\cdot\boldsymbol{u}'\\
H_2 &= \frac{(p')^2}{2\gamma\rho_0 P_0}+\frac{(u')^2}{2}\\
H_3 &= \frac{(\gamma+1)}{6\gamma^2 P_0^2\rho_0}(p')^3
\end{aligned} \tag{12}$$

and the mass flux to various orders is given by

$$\begin{aligned}
\boldsymbol{m}_1 &= \rho_0\boldsymbol{u}'+\frac{\boldsymbol{U}_0}{a_0^2}p'\\
\boldsymbol{m}_2 &= \frac{p'\boldsymbol{u}'}{a_0^2}+\boldsymbol{U}_0\frac{(1-\gamma)}{2\gamma a_0^2 P_0}(p')^2\\
\boldsymbol{m}_3 &= \frac{\rho_0(1-\gamma)}{2\gamma^2 P_0^2}\boldsymbol{u}'(p')^2+\boldsymbol{U}_0\frac{(1-\gamma)(1-2\gamma)}{6\gamma^2 a_0^2 P_0^2}(p')^3
\end{aligned} \tag{13}$$

The energy density $E$ is also a nonlinear function of wave amplitude; thus $E'$, the fluctuating part or acoustic energy density, is expanded as

$$E'=\epsilon^2 E_1+\epsilon^3 E_2+\epsilon^4 E_3+\ldots \tag{14}$$

The series begins with a term proportional to $\epsilon^2$ since the linear acoustic energy is of quadratic form. Multiplication of the continuity equation (7) by $H'$ and combining with the scalar product of the momentum with $\boldsymbol{m}'$ yields the required energy balance equation

$$\frac{\partial E'}{\partial t}=-\nabla\cdot(H'\boldsymbol{m}') \tag{15}$$

For the present case there are no production terms because of the following set of assumptions: 1) irrotational flow, 2) uniform mean pressure, 3) retention of mean flow terms only to $\mathcal{O}(M_b)$, 4) no combustion within the volume of the chamber (all viscous and thermal nonuniformity is confined to a thin region near the burning surfaces), and 5) volume losses such as those due to regions of nonuniformity in steep wave fronts (nonisentropic losses) are confined to zones of negligible thickness which can be treated as discontinuities. It is clear that some phenomena affected by these assumptions are therefore not properly addressed. Incorporation of rotational flow effects, turbulence, or large-scale vortex formation is not attempted in the present effort.

It is now possible to identify the components of the acoustic energy density expansion to third-order accuracy. Expanding the left side of Eq. (15) and inserting the $H'$ and $\boldsymbol{m}'$ expansions, one finds

$$E_1=\rho_0\left(\frac{\boldsymbol{u}'\cdot\boldsymbol{u}'}{2}\right)+\frac{\boldsymbol{U}_0\cdot\boldsymbol{u}'}{a_0^2}p'+\frac{(p')^2}{2\gamma P_0} \tag{16}$$

$$E_2=p'\left(\frac{\boldsymbol{u}'\cdot\boldsymbol{u}'}{2a_0^2}\right)+\frac{(1-\gamma)\boldsymbol{U}_0\cdot\boldsymbol{u}'}{2\rho_0 a_0^4}(p')^2+\frac{(1-2\gamma)}{6\rho_0^2 a_0^4}(p')^3 \tag{17}$$

$$E_3=\left[\frac{(1-\gamma)}{4\gamma a_0^2 P_0}\right](p')^2(\boldsymbol{u}'\cdot\boldsymbol{u}')+\frac{(1-\gamma)(1-2\gamma)\boldsymbol{U}_0\cdot\boldsymbol{u}'}{6\gamma^2 a_0^2 P_0^2}(p')^3+\frac{(1-3\gamma)(1-2\gamma)}{8\gamma^3 P_0^3}(p')^4 \tag{18}$$

Except for the mean flow interaction term in Eq. (16), $E_1$ is the classical energy density as in the linear analysis. The second term has been the focus of much controversy; it will be demonstrated that this term is correctly placed and does not lead to results inconsistent with solutions of the linear problem carried out by other means. Each of the components of the energy expansion consists of rapidly fluctuating and slowly varying parts. Of primary interest is an estimate of the rate of change of the time-averaged system energy since, as already demonstrated, this provides a means for assessing the nonlinear stability of the system. Taking the time average of Eq. (15), and integrating over the chamber volume to determine the global rate of change of the system energy

$$\frac{\partial}{\partial t}[\epsilon^2(\mathrm{E}_1+\epsilon\mathrm{E}_2+\epsilon^2\mathrm{E}_3+\ldots)]=-\int_V\langle\nabla\cdot(H'\boldsymbol{m}')\rangle\mathrm{d}V \tag{19}$$

where

$$\mathrm{E}_n=\int_V\langle E_n\rangle\mathrm{d}V \tag{20}$$

is the time-averaged system energy to order $n$. As a result of the assumption that the waveform is frozen, the only remaining function of time is represented by the slowly changing composite amplitude $\epsilon$. Solving Eq. (19) for the rate of change of $\epsilon$,

$$\frac{\mathrm{d}\epsilon}{\mathrm{d}t}=\frac{-\int_V\langle\nabla\cdot(H'\boldsymbol{m}')\rangle\mathrm{d}V}{\epsilon(2\mathrm{E}_1+3\epsilon\mathrm{E}_2+4\epsilon^2\mathrm{E}_3+\ldots)} \tag{21}$$

Defining the nonlinear acoustic intensity,

$$I'=\langle H'\boldsymbol{m}'\rangle=\epsilon^2 I_1+\epsilon^3 I_2+\epsilon^4 I_3+\ldots \tag{22}$$

the intensity components are found to be

$$I_1 = \left\langle p'u' + \frac{U_0(p')^2}{\rho_0 a_0^2} + \rho_0 u'(U_0 \cdot u') \right\rangle + \mathcal{O}(M_b^2) \tag{23}$$

$$I_2 = \left\langle \frac{\rho_0}{2} u'(u' \cdot u') - \frac{U_0(p')^3}{2a_0^2 \gamma P_0^2} + \frac{u'(U_0 \cdot u')p'}{2a_0^2} + \frac{u'(p')^2}{2\gamma P_0} \right\rangle \tag{24}$$

$$I_3 = \left\langle \frac{(1-2\gamma)}{6\gamma^2 P_0^2} u'(p')^3 + \frac{p'u'(u' \cdot u')}{2a_0^2} + \frac{(1-\gamma+4\gamma^2)}{12\gamma^3 P_0^3} U_0(p')^4 + \frac{3(1-\gamma)(U_0 \cdot u')}{4\gamma a_0^2 P_0}(p')^2 u' \right\rangle \tag{25}$$

The volume integral in Eq. (21) can be converted directly to a surface integral by means of Green's theorem, thus

$$\int \langle \nabla \cdot (H'm') \rangle \mathrm{d}V = \int \langle n \cdot I' \rangle \mathrm{d}S \equiv -(\epsilon^2 \eta_1 + \epsilon^3 \eta_2 + \epsilon^4 \eta_3 + \ldots) \tag{26}$$

where

$$\eta_n = -\int n \cdot I_n \mathrm{d}S \tag{27}$$

It is useful to employ the mean flow Mach number as the small parameter in a second perturbation expansion. For example, the first-order energy can be written as

$$\mathrm{E}_1 = \mathrm{E}_0(1 + M_b F) \tag{28}$$

where $\mathrm{E}_0$ is the classical linear acoustic energy

$$\mathrm{E}_0 = \int_V \left\langle \frac{p'^2}{2\gamma P_0} + \rho_0 \frac{u' \cdot u'}{2} \right\rangle \mathrm{d}V \tag{29}$$

and $M_b F$ is the mean flow correction with

$$F = \frac{1}{\mathrm{E}_0} \int_V \left\langle \frac{U(r) \cdot u' p'}{a_0} \right\rangle \mathrm{d}V \tag{30}$$

The mean flow vector $U_0 = v_b U(r)$ has been written in terms of normal influx speed at the burning surface; the reference mean flow Mach number is conveniently defined to be $M_b = v_b/a_0$. Taking $M_b$ to be a small parameter, the denominator in Eq. (21) can now be inverted and expanded in a double perturbation series. Thus

$$[2\mathrm{E}_1 + \epsilon(3\mathrm{E}_2 + 4\epsilon^2 \mathrm{E}_3)]^{-1} = \frac{1}{2\mathrm{E}_1}\left\{1 + \epsilon\left(\frac{-3\mathrm{E}_2}{2\mathrm{E}_1}\right) + \epsilon^2\left[\frac{9}{4}\left(\frac{\mathrm{E}_2}{\mathrm{E}_1}\right)^2 - \frac{2\mathrm{E}_3}{\mathrm{E}_1}\right] + \ldots\right\} \tag{31}$$

with the factor

$$\tfrac{1}{2}\mathrm{E}_1 = [1 - M_b F + \mathcal{O}(M_b^2)]/2\mathrm{E}_0 \tag{32}$$

Finally, the expression for the rate of change of the composite system energy may be written in the useful form

$$\frac{\mathrm{d}\epsilon}{\mathrm{d}t} = \epsilon A + \epsilon^2 B + \epsilon^3 C + \mathcal{O}(\epsilon^4) \tag{33}$$

which clarifies the origins of limiting and triggering behavior as will be demonstrated. Each of the coefficient functions on the right of Eq. (33) can now be evaluated. These are expressions involving volume and surface integrals over the chamber domain. Before doing this, it is necessary to determine the correction terms that account for steep fronted wave effects. As the analysis stands, these losses have not been accounted for because of the isentropic flow assumption. It is proper simply to add the shock losses to the integral results because they occur in a very thin region in which the temperature and density gradients are very high. This region may be treated mathematically as a discontinuity, and the flow on either side of the shock wave can be assumed isentropic; thus the shock energy loss can be directly superimposed on the integral results.

## Energy Loss in Shock Fronts

Energy dissipation in shock waves has long been recognized as a potentially important contribution to the system behavior (cf. Refs 14-21). When finite waves appear in a lightly damped system, nonisentropic mechanisms arise naturally to limit the system amplitude. It is sometimes the case that the harmonics are heavily damped by particulate damping or similar effects. Then steepening may not occur, although finite amplitudes are present. The analysis presented here allows either situation; if the harmonics are not strongly damped, then steep wave fronts may form and it is necessary to include in the model an estimate for their effect on the rate of change of composite amplitude. Experimental data occasionally suggest the presence of more than one shock front. Two or more steep waves with arbitrary phase can be superimposed using the methods described in this paper; it is then necessary to account for the additional entropy generation and associated energy flux. Only a single wave is analyzed here since, for the majority of the experimental data considered, multiple waves were clearly not present.

The first inclusion of shock losses in rocket instability analysis appears to have been carried out by Temkin.[21] His estimate, like that of subsequent investigators, was based on classical gasdynamics. The energy loss per unit area of the wave front is

$$\left(\frac{\mathrm{dE}}{\mathrm{d}t}\right)_{\text{shock}} = -\epsilon^3 \frac{(\gamma+1)}{12\gamma^3} \rho_0 a_0^3 \tag{34}$$

This result must be extended to fourth order in wave amplitude to make it compatible with the nonlinear energy balance equation. The average rate of energy dissipation for

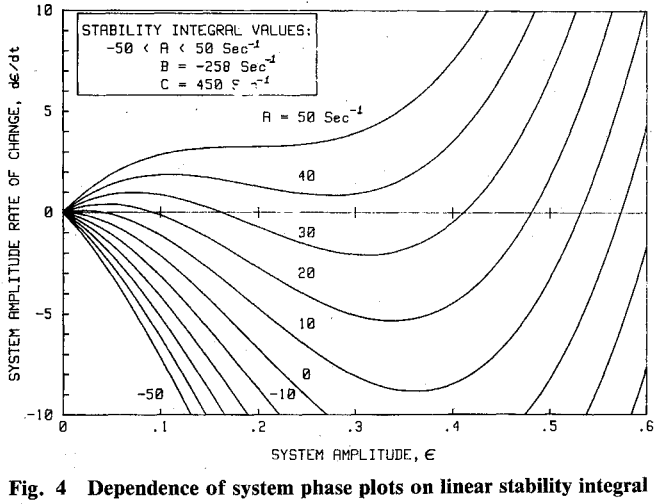


Fig. 4 Dependence of system phase plots on linear stability integral $A$.

a planar traveling discontinuity can be written as

$$\left(\frac{dE}{dt}\right)_{shock} = S_{front}\rho_0 a_0 T_0 (s-s_0) \tag{35}$$

where $(s-s_0)$ is the entropy increase across the region of nonuniformity. The entropy change can be estimated by means of fundamental thermodynamic principles to be

$$(s-s_0) = c_v \ell n[(p/P_0)(\rho/\rho_0)^\gamma] \tag{36}$$

and by application of the Rankine-Hugoniot relations,

$$(s-s_0) = c_v\left\{\ell n\left(1+\frac{p'}{P_0}\right)\left[1+\left(\frac{p'}{P_0}\right)\frac{(\gamma-1)}{2\gamma}\right]^\gamma - \ell n\left[1+\left(\frac{\rho'}{P_0}\right)\frac{(\gamma-1)}{2\gamma}\right]^\gamma\right\} \tag{37}$$

Thus, to fourth order in $\epsilon$, the rate of change of composite energy assuming a single wave front is given by

$$\left(\frac{d\epsilon}{dt}\right)_{shock} = \frac{1}{2E_0}\left(\frac{dE}{dt}\right)_{shock} = \left(\frac{a_0}{L}\right)\left(\frac{\gamma+1}{8\xi\gamma}\right)\left[-\frac{\epsilon^2}{3}+\frac{\epsilon^3}{2}-\frac{\epsilon^4}{20\gamma^2}(11\gamma^2+1)+\ldots\right] \tag{38}$$

which extends the classical theory beyond the accuracy required. Figure 3 shows plots of this expression and the effects of truncation of the series. Note that the $\mathcal{O}(\epsilon^3)$ correction is positive while the $\mathcal{O}(\epsilon^2)$ and $\mathcal{O}(\epsilon^4)$ terms are negative. Since $\epsilon$ is small, the net energy rate is negative as required; the shock loss expansion does not converge particularly rapidly. It is interesting that the second term taken by itself seems to imply an energy source at this order; this behavior is typical of asymptotic representations and, of course, must not be interpreted without due consideration of the presence of the other terms in the series. Other gasdynamic interactions in the nonlinear rocket instability analysis display similar alternating signs. Great care must be exercised in constructing physical interpretations of the mathematical results. Great conceptual difficulties can arise if one talks of "second-order energy gains and losses" in the same sense that is used in discussions of the linear gain/loss balance. The second-order and subsequent terms in the series expansions must be interpreted as corrections to the corresponding linear terms. Thus, the positive third-order shock-wave energy flux in reality indicates that the second-order shock-wave energy loss is smaller than that calculated from a representation using only the leading term. Again, at the amplitudes typical of nonlinear rocket motor oscillations ($\epsilon \sim 0.3$), significant modification of the nonisentropic energy loss is introduced by the higher-order corrections.

## Interpretation of Results

It is now possible to examine the results of the analysis in terms of its physical content. This is best accomplished by examination of the integral terms on the right of Eq. (33). It is a consequence of the assumed fixed waveform that the function $F$ (the Blokhintsev/Cantrell/Hart correction to the linear acoustic energy density) is zero. Thus functions $A$, $B$, and $C$ are readily evaluated; the shock-wave corrections are included with the proviso that they are to be set to zero for cases where no steep fronts are present. $A$ is shown to be equivalent to the classical linear stability integral. $B$ and $C$ will be referred to, respectively, as the second- and third-order nonlinear stability integrals.

The linear system is governed by

$$A = -\left(\frac{1}{2E_0}\right)\int_s \left\langle n\cdot\left[u'p' + (U_0\cdot u')u'\rho_0 + U_0\frac{p'^2}{\gamma P_0}\right]\right\rangle dS \tag{39}$$

The term $U_0\cdot u'$ evaluated at the burning surface is of order $M_b^2$ since $U_0\cdot u' = v_b n\cdot u'$ is of order $M_b^2$. Thus this term must be dropped since only terms that are linear in the mean flow Mach number have been retained throughout the analysis. Thus one finds

$$A = \alpha = -\left(\frac{1}{2E_0}\right)\int_s \left\langle n\cdot\left(u'p' + U_0\frac{p'^2}{\gamma P_0}\right)\right\rangle dS \tag{40}$$

where $\alpha$ is the linear growth rate as derived in many previous analyses (cf. Culick[13]). Thus function $A$ can be replaced by the linear growth rate determined from any appropriate computer program. The first term in the integral is the source of combustion energy flow into the oscillatory system. Great care must be taken in the handling of this term. Since the combustion response is itself a nonlinear process, the expression $n\cdot u'p'$ evaluated at the burning surface may introduce higher-order effects, which must be shifted to the $B$ and $C$ or higher-order integrals according to their dependence on the system amplitude. These corrections are introduced in the course of evaluating and simplifying the stability integrals.

Before further appraisal of the stability integrals is undertaken, some discussion of velocity coupling effects is in order. It is assumed that velocity coupling in its classical form is not present. To introduce a velocity coupled response as an ad hoc correction to the stability integrals, for example, as an additional term in $A$ of the form $n\cdot u'|u'|$, would be inconsistent with the analysis. Such artificial incorporation of velocity-dependent combustion effects has been a common stratagem to add additional degrees of freedom for the fitting of experimental data. If such terms were necessary or appropriate, they would automatically appear in the mathematical development. Since velocity coupling has often been invoked as a means for explaining nonlinear rocket behavior, it is of considerable interest to determine if a model based entirely on expansions of the fundamental conservation equations can give rise to nonlinear processes such as limiting and triggering. Many of the characteristics of nonlinear behavior often attributed to velocity coupling will be shown to arise in a natural way as combustion corrections of second and third order without the need for ad hoc velocity coupling models. The dependence of the unsteady energy flux on the velocity fluctuations and on the mean flowfield are demonstrated to be of precisely the form anticipated by various ad hoc models. An observation of the greatest significance is that the velocity coupling corrections enter the problem as nonlinear correction terms. This is in keeping with the hypothesis that there cannot be a linear velocity coupling effect analogous to the linear pressure coupling phenomenon.

Using the conventional definition of the combustion response function, one writes

$$R_b = \frac{m'/m_0}{p'/P_0} \tag{41}$$

where $m'$ is the fluctuating mass flow rate crossing the system boundary at the edge of the combustion zone. Since we are dealing with a nonlinear problem, it is necessary to allow for a nonlinear interpretation of Eq. (41). That is, $R_b$ must include corrections to the same order as the complete analysis is carried Using the expansion method employed in

the general analysis, the response can be written as

$$R_b = R_b^{(1)} + \epsilon R_b^{(2)} + \epsilon^2 R_b^{(3)} + \ldots \tag{42}$$

where the functions $R_n^{(n)}$ must be taken to be complex numbers to allow for the possiblity that the normal velocity response to the incident wave might be out of phase with local pressure fluctuations; for the linear part of the problem, only the real part of $R_b^{(1)}$ contributes a net average energy flux to the waves. This may not be true for the nonlinear corrections, so care must be taken not to disregard potentially important terms. The response constants used in what follows are to be taken as the part of the complex function that yields a normal velocity fluctuation in phase with (or 180 deg out of phase with) the local pressure oscillations at the edge of the flame. No special notation will be carried along to highlight this interpretation unless it is required for clarity. The response function components are expanded with the assumption of isentropic flow within the chamber (that is, outside the combustion zone). The results are

$$R_b^{(1)} = \left(\frac{v^{(1)} v_b}{p'/P_0} + \frac{1}{\gamma}\right)$$

$$R_b^{(2)} = \left(\frac{v^{(2)}/v_b}{p'/P_0} + \frac{v^{(1)}/v_b}{\gamma} - \frac{(\gamma-1)}{2\gamma^2}\frac{p'}{P_0}\right)$$

$$R_b^{(3)} = \left[\frac{v^{(3)}/v_b}{p'/P_0} + \frac{v^{(2)}/v_b}{\gamma} - \frac{(\gamma-1)}{2\gamma^2}\frac{p'}{P_0}\frac{v^{(1)}}{v_b} - \frac{(1-\gamma)(1-2\gamma)}{6\gamma^3}\left(\frac{p'}{P_0}\right)^2\right] \tag{43}$$

and each of these expressions can be solved for the normal velocity response for each level of approximation with the result

$$v^{(1)} = (\boldsymbol{n}\cdot\boldsymbol{u}')_1 = -v_b\left(\frac{p'}{P_0}\right)\left(R_b^{(1)} - \frac{1}{\gamma}\right) \tag{44}$$

$$v^{(2)} = (\boldsymbol{n}\cdot\boldsymbol{u}')_2 = -v_b\left(\frac{p'}{P_0}\right)\left[R_b^{(2)} - \frac{1}{\gamma}\frac{v^{(1)}}{v_b} + \frac{(\gamma-1)}{2\gamma^2}\left(\frac{p'}{P_0}\right)\right] \tag{45}$$

$$v^{(3)} = (\boldsymbol{n}\cdot\boldsymbol{u}')_3 = -v_b\left(\frac{p'}{P_0}\right)\left[R_b^{(3)} - \frac{1}{\gamma}\frac{v^{(2)}}{v_b} + \frac{(\gamma-1)}{2\gamma^2}\left(\frac{p'}{P_0}\right)\frac{v^{(1)}}{v_b} - \frac{(1-\gamma)(1-2\gamma)}{6\gamma^3}\left(\frac{p'}{P_0}\right)^2\right] \tag{46}$$

Thus the linear contribution from combustion is

$$\int_{S_b} -\boldsymbol{n}\cdot\boldsymbol{u}'p'\,\mathrm{d}S = \int_{S_b} v_b\left(R_b^{(1)} - \frac{1}{\gamma}\right)\frac{p'^2}{P_0}\,\mathrm{d}S \tag{47}$$

and finally the complete linear stability integral can be written as

$$A = \left(\frac{1}{2\mathrm{E}_0}\right)\left\langle \int_{S_b} v_b R_b^{(1)}\frac{p'^2}{P_0}\mathrm{d}S - \int_{S_n} v_n(1+A_n)\frac{p'^2}{\gamma P_0}\mathrm{d}S\right\rangle \tag{48}$$

where $v_n$ and $A_n$ are the normal mean flow velocity and the admittance funtion at the nozzle entrance. $S_b$ and $S_n$ refer to integration over the burning propellant surfaces and the nozzle entrance region, respectively. Only a linear nozzle model is incorporated; nonlinear terms could be introduced in the same manner as displayed for the combustion effects. The nonlinear terms $(\boldsymbol{n}\cdot\boldsymbol{u}')_2$ and $(\boldsymbol{n}\cdot\boldsymbol{u}')_3$ must be shifted into the integrals $B$ and $C$ in accordance with the ordering scheme used throughout the analysis. The linear approximation given in Eq. (48) is completely consistent with previously accepted combustion instability analyses.

Now consider the second-order nonlinear behavior as represented by integral $B$. If the second-order shock-wave loss is included, $B$ takes the form

$$B = -\left(\frac{1}{2\mathrm{E}_0}\right)\int_S \left\langle \boldsymbol{n}\cdot\boldsymbol{u}'\left(\rho_0\frac{\boldsymbol{u}'\cdot\boldsymbol{u}'}{2} + \frac{p'^2}{\gamma P_0}\right)\right\rangle \mathrm{d}S + \int_S \left\langle \boldsymbol{n}\cdot\boldsymbol{U}_0\left(\frac{\boldsymbol{u}'\cdot\boldsymbol{u}'p'}{2a_0^2} - \frac{p'^3}{2\gamma P_0^2}\right)\right\rangle \mathrm{d}S + \left(\frac{3\mathrm{E}_2}{2\mathrm{E}_1}\right)\int\left\langle \boldsymbol{n}\cdot\boldsymbol{u}'p' + \boldsymbol{n}\cdot\boldsymbol{U}_0\frac{p'^2}{\gamma P_0}\right\rangle \mathrm{d}S + \int_{S_b}\langle(\boldsymbol{n}\cdot\boldsymbol{u}')_2 p'\rangle \mathrm{d}S - \left(\frac{1}{\epsilon}\right)\left(\frac{\mathrm{dE}}{\mathrm{d}t}\right)^{(2)}_{\text{shock}} \tag{49}$$

where the nonlinear combustion term to second order has been incorporated as explained. Use of the frozen waveform assumption results in further simplification since several of the resulting integral terms vanish in the process of time averaging. One is left with

$$B = \frac{1}{2\mathrm{E}_0}\int_{S_b}\left\langle v_b R_b^{(1)}\left(\frac{\rho_0 p^*\boldsymbol{u}'\cdot\boldsymbol{u}'}{2P_0} + \frac{p'^2 p^*}{\gamma P_0^2}\right)\right\rangle \mathrm{d}S + \frac{1}{2\mathrm{E}_0}\int_{S_b}\left\langle v_b\left(\frac{p'^2}{P_0}\right)\left(R_b^{(2)} + \frac{p^* R_{bi}^{(1)}}{\gamma P_0}\right)\right\rangle \mathrm{d}S - \left(\frac{a_0}{L}\right)\frac{(\gamma+1)}{24\xi\gamma} \tag{50}$$

where $p^*$ is the complex conjugate of $p'$. Subscript $i$ refers to the imaginary part. This indicates the potential importance of nonlinear combustion response as represented by the term $R_b^{(2)}$. The shock-wave loss dominates this set of terms in cases where a steep wave front is present. Inspection of the combustion terms reveals that the dependence on the linear part of the combustion repsonse function involves the imaginary part of the response function. The dependence of this term on the velocity fluctuations is quite similar to that used in some velocity coupling models; it is significant that such terms arise naturally as part of the second-order corrections. Velocity coupling does not appear in the first-order formulation unless it is inserted artificially. Nonlinear nozzle

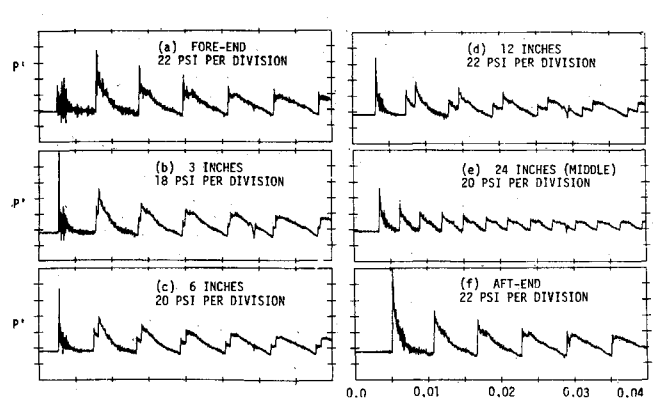


**Fig. 5 Experimental pulse decay data due to Lovine.[3]**

terms could be incorporated in similar fashion, but since there is not complete agreement on nozzle loss models, only linear nozzle contributions are addressed. The conventional short nozzle approximation will be used in the numerical evaluations. Notice that the shock loss term depends inversely on motor length. The second-order combustion response can contribute a system energy loss or a net gain since each of the two response function terms can have either sign.

Third-order system energy contributions are represented by the function $C$, which is handled in a manner similar to that just described for the second-order effects. The result is

$$C=\frac{(\gamma+1)a_0}{16\gamma\xi}+\left(\frac{a_0}{L}\right)\left(\frac{E_3}{E_0^2}\right)J\left(\frac{2}{(\gamma+1)}\right)^{\frac{(3-\gamma)}{2(\gamma-1)}}$$
$$+\left(\frac{v_b}{2E_0P_0}\right)\left[\int_{S_b}\left(\frac{3(3\gamma-5)}{4\gamma^3}+\frac{(16-5\gamma)R_b^{(1)}}{6\gamma^2}\right)\frac{\langle p'^4\rangle}{P_0^2}dS\right.$$
$$+\left(\frac{1}{a_0^2}\right)\int_{S_b}\left(\frac{(\gamma-5)}{4\gamma}+R_b^{(1)}\right)\langle u'\cdot u'p'^2\rangle dS$$
$$\left.-\left(\frac{E_3}{E_0}\right)\int_{S_b}R_b^{(1)}\langle p'^{(2)}\rangle dS\right]$$
$$-\left(\frac{v_n}{2E_0}\right)\int_{S_n}\left[\frac{3(3\gamma-5)}{4\gamma^3}+\frac{(16-5\gamma)A_n}{6\gamma^2}\right]\langle p'^4\rangle dS \quad (51)$$

where, again, the nonlinear combustion terms of appropriate order have been shifted from both the first- and second-order acoustic intensity integrals and the third-order shock loss term has been appended.

Since reliable nonlinear response function data are not yet available, and even reliable linear data are difficult to obtain, it is appropriate to ignore the nonlinear response function terms. The linear response is represented in the next section of the paper by actual propellant data. It is of considerable interest to determine whether or not the linear pressure coupled terms, with their associated nonlinear corrections proportional to the linear response function, can give rise to the nonlinear attributes usually associated with velocity coupling or other nonlinear phenomena. Many potentially interesting terms are not displayed in the results shown. For instance, no attempt is made to present nonlinear nozzle terms or effects of nonlinear two-phase interactions due to the presence of particulate matter. Losses at inert surfaces are also not displayed but were included in the burner simulations to be described later. Other processes can be incorported by application of the same procedures employed for the combustion and shock effects. The results shown can be enhanced as necessary with these other effects by simply adding the integral contributions. The integrals at each order are made up of terms that are linearly additive because the perturbation expansion process renders the nonlinear problem into a set of linear ones.

Solutions are carried out by evaluating the three stability integrals $A$, $B$, and $C$. Sensitivity studies are readily performed by varying combinations of the input parameters and geometrical variables. Results for a given situation can be displayed as shown in Fig. 4 as plots of the rate of change of wave amplitude vs the global system amplitude, that is, by plotting Eq. (33) with the resulting values for the stability functions. In Fig. 4, typical values for the functions for a sonic end-vent burner configuration are utilized. The vitally important role of the linear stability integral is emphasized by holding the values of the second- and third-order integrals fixed and varying $A$ over a typical range. For a linearly stable system ($A<0$), the system response to moderate pulses is the expected decay ($d\epsilon/dt<0$). Only if a large pulse is applied ($\epsilon>\epsilon_{trigger}$) will there be significant response under these conditions. Notice that the trigger amplitude predicted by the analysis for negative values of $A$ are quite large, say, of the order of 0.5, which is larger than pulses commonly used in testing of burners or motors. Thus, for the situation illustrated, only linearly unstable systems are of practical concern. This partially justifies the common belief in the linear stability analysis as a means of avoiding combustion instability problems in practice; as long as the system is linearly stable, only a very large pulse (for the conditions illustrated) could result in oscillations of growing amplitude. One must be cognizant of the possiblity that the triggering amplitude might be lower than those displayed under some conditions. In such a case, only a moderate pulse might cause an otherwise stable system to become unstable.

Again referring to Fig. 4, as positive values of $A$ are introduced, a stable limit cycle appears. For $A\equiv 0$, this is a trivial limit cycle of amplitude 0. It is of interest to note that the origin, $\epsilon=0$, is also a trivial triggering amplitude for the linearly unstable case; that is, a pulse of zero amplitude initiates the growth of the system toward a yet higher amplitude. As the value of $A$ is increased, the limiting amplitude that can be sustained by the system rises and the second triggering amplitude decreases. At a critical combination of parameters, the limit cycle and the second triggering point converge, and there are no further singular points (assuming third-order accuracy). Higher values of $A$ simply increase the rate at which the composite amplitude grows in time; the system is then truly unstable (to third-order accuracy) since it will grow without limit. Higher-order analyses are required if additional limit and triggering singular points must be considered.

The third-order analysis, as presented here, is the lowest order at which true triggering effects appear. On the basis just described, a true triggering amplitude can be defined without ambiguity as a nonzero composite system amplitude above the lowest limit cycle amplitude which is an unstable zero of $d\epsilon/dt$. Pulsing the system above this amplitude causes divergence to a yet higher composite amplitude. It is suggested that the trivial triggering amplitude (at $\epsilon_{trigger}=0$) for linearly unstable systems not be treated in interpretation of experimental data as triggering in the true sense. Pulsing below the limit amplitude does obviously hasten the growth of the system to the limit cycle; the curves of Fig. 4 clarify the reasons for this. There is an optimum pulse amplitude below $\epsilon_{limit}$ which maximizes the rate of change of global amplitude. True triggering involves growth of the system to an amplitude beyond the lowest limit cycle point; it is this sort of behavior that must be understood and avoided in operational rocket motors.

## Applications

The analysis is now applied to several test cases to determine its characteristics and applicability to the nonlinear rocket instability problem. Configurations based on actual experiments are analyzed; the situations arising in a recent Air Force sponsored study[5] are emphasized. These are presented in order of increasing complexity, starting with measurements made in cold flow pulser simulations and progressing to multiple-grain burner configurations.

A closed chamber without combustion or mean flow represents a useful starting point since this case has been used in the evaluation of other analyses. The recent experiments of Lovine[4] are utilized here. Tests were performed using a cylindrical chamber 1.22 m (48 in.) long and 0.077 m (3.056 in.) in diameter. The chamber which initially contained nitrogen at 100 psi was pulsed into oscillation by a pyrotechnic device located at one end. Levine, Baum, and Lovine[3] discuss the numerical assessment of these test data. It is useful to compare the predictions of their elaborate numerical technique to the analytical method presented here. Figure 5 shows Lovine's pressure traces taken simultaneously at several points in the chamber.

If viscous losses are neglected, the evaluations of the integrals $A$, $B$, and $C$ are easily carried out and the system

behavior is governed by

$$\frac{d\epsilon}{dt}=\epsilon^2\left\{\left(\frac{a_0}{L}\right)\left(\frac{\gamma+1}{8\xi\gamma}\right)\left[-\frac{1}{3}+\frac{\epsilon}{2}+\epsilon^2\frac{(11\gamma^2+1)}{20\gamma^2}\right]\right\} \quad (52)$$

where the nonisentropic steep wave loss has been represented to fourth-order accuracy. This simple nonlinear differential equation for the wave amplitude envelope can be readily solved by numerical integration. Results are shown in Fig. 6. Equation (1), with the spectral coefficients of Eq. (5), was used to approximate the waveform. The measured pressure information is extremely complicated at the pulse initiation, as would be expected during the initialization of the waves; obviously the analysis cannot properly represent the initial transient since only slow global amplitude changes are addressed. It is apparent, however, that the analysis describes the post-transient properties of the experiments with considerable fidelity. The initial amplitude used in the analytical solution was scaled from the measured value at the fore end of the chamber. The predicted decay rate matches the experimental data very closely and yields essentially the same quality of information as the completely numerical analysis described in Ref. 4.

Of great practical interest is the application of the results to systems with combustion. The geometry and system parameters used in the following numerical evaluations are based on the sonic end-vent tests carried out by Micheli and Lovine as part of a recent Air Force program.[5] A simple tubular chamber with one or more arbitrarily placed cylindrical grain elements and a choked end-vent nozzle is assumed; Fig. 1 illustrates a typical configuration. The experimental apparatus allowed up to three pulses to be introduced during each run. The second pulse was usually timed to correspond to the point in time at which the grain samples become flush with the inside surface of the tube. These conditions correspond to the most unstable configuration observed during the testing; thus, it is appropriate to assume this geometry for analysis. Actual propellant data were utilized to represent the linear combustion response function $R_b^{(1)}$. For this set of assumptions, one finds

$$A=\frac{\gamma v_b}{2\dot{R}\xi}\int_{S_b}\sum_{n=1}^{\infty}R_b^{(1)}\cos k_n\left(\frac{x}{L}\right)dx-\left(\frac{a_0}{L}\right)J\left(\frac{2}{\gamma+1}\right)^{\frac{(3-\gamma)}{2(\gamma-1)}} \quad (53)$$

$$B=-\left(\frac{a_0}{L}\right)\left(\frac{\gamma+1}{24\xi\gamma}\right) \quad (54)$$

$$C=\left(\frac{a_0}{L}\right)\left[\frac{\gamma+1}{16\gamma\xi}+J\left(\frac{2}{\gamma+1}\right)^{\frac{3-\gamma}{2(\gamma-1)}}\left(\frac{2E_3}{E_0}\right)\right]+v_b\left(\frac{\gamma}{2VP_0^2\xi}\right)\left[\left(\frac{I_1}{P_0^2}\right)+\left(\frac{I_2}{a_0^2}\right)-\left(\frac{E_3}{E_0}\right)I_0\right]+\left(\frac{a_0}{L}\right)\left[\frac{(5\gamma^3-21\gamma^2-11\gamma+45)}{24\xi\gamma^2}\right]I_3J\left(\frac{2}{\gamma+1}\right)^{\frac{\gamma+1}{2(\gamma-1)}} \quad (55)$$

where the integrals are defined by

$$I_0=\int_{S_b}\langle R_b^{(1)}(p')^2\rangle dS$$

$$I_1=\int_{S_b}\left\langle\left[\frac{3(3\gamma-5)}{4\gamma^2}+\frac{(16-5\gamma)}{6\gamma^2R_b^{(1)}}\right]p'^4\right\rangle dS$$

$$I_2=\int_{S_b}\left\langle\left[\frac{(\gamma-5)}{4\gamma}+R_b^{(1)}\right]u'\cdot u'p'^2\right\rangle dS$$

$$I_3=\int_{S_n}\langle p'^4\rangle dS \quad (56)$$

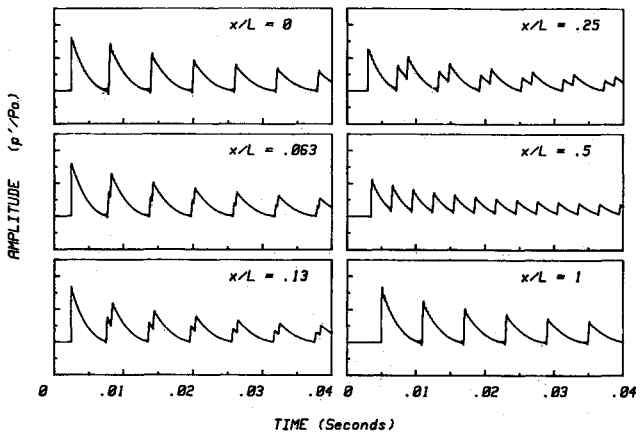


Fig. 6 Analytic pulse decay simulating Lovine experiment.

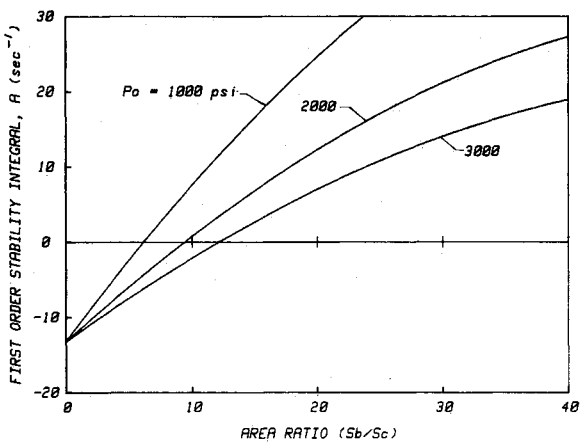


Fig. 7 Sensitivity of linear stability integral to area ratio: simulated sonic end-vent burner.

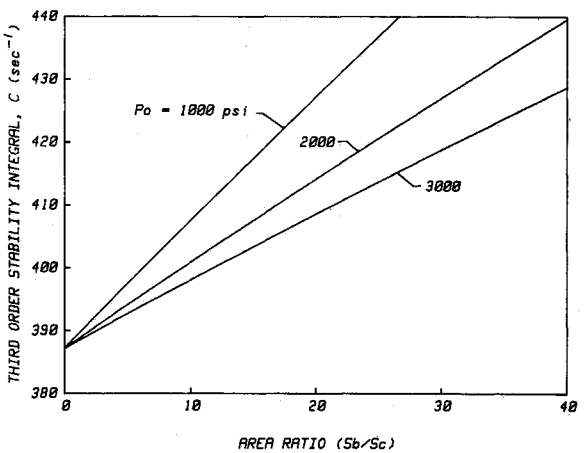


Fig. 8 Sensitivity of third-order stability integral to area ratio: simulated sonic end-vent burner.

Notice the appearance of the response function within the integrals. Since $R_b^{(1)}$ is strongly frequency dependent, it must be treated as a weighting function in the Fourier expansions for $p'$ and $u'$. A sharply peaked response function will tend to emphasize the effect of a mode located near the peak. The integrals require numerical evaluation; the third-order integrals require considerable computer time if they are recomputed for every case. Consequently, it was found advantageous to determine a set of solutions covering a wide range of grain lengths, number of grains, and grain locations. These were replaced by accurate polynomial functions stored

as disk files. Parameter studies involving numerous computations of system behavior were thereby greatly facilitated. Some examples of the results are briefly discussed here. Using geometrical values representative of sonic end-vent burner tests (typically, chamber length of 1.21 m and diameter of 0.038 m with a mean pressure of 2257 psia, $\gamma = 1.19$, two grains of length 0.238 m located at each end), one finds for the stability functions: $A = 24$, $B = -261$, $C = 396$ in units of $s^{-1}$. The limit amplitude for oscillations that grow incipiently or start from a pulse lower than the limit cycle amplitude is found by solving Eq. (33) for its stable singular point with the result $\epsilon_{limit} = 0.11$. For the values of the stability integrals displayed, the system exhibits true triggering. That is, there is an unstable singular point at an amplitude of $\epsilon_{trigger} = 0.55$. The latter amplitude is well above those that might be observed in practical situations. The predicted limiting amplitude, however, is quite typical of the observations. The case in question is linearly unstable; that is, $A$ is a positive number and the oscillations grow incipiently.

The values for $B$ and $C$ are strongly dominated by the shock losses. Figures 7 and 8 show the sensitivity of $A$ and $C$ to the mean operating pressure $P_0$ and the ratio of the burning surface to the chamber cross-sectional area. For the common circumstance in which the system is linearly stable ($A < 0$), the turning point at $\epsilon = 0$ is stable and may be interpreted as a "limit cycle" amplitude of zero. In this situation the next higher singular point of Eq. (33) is a triggering point, as illustrated in Fig. 4; if the system amplitude is pulsed to a value above this, the amplitude grows without bound. When $A$ is positive (linearly unstable case), $\epsilon = 0$ may be considered as a trivial triggering amplitude; the system is "triggered" and grows incipiently. In this case, the next critical system amplitude is a stable limit cycle and the next higher singular point is a true triggering amplitude.

A series of computations was carried out to determine if the analysis yields sensitivity trends similar to those observed in practice. Figure 9 shows the effects of area ratio and mean pressure on the limit cycle amplitude. Very similar plots were generated in the course of analyzing the experimental data.[5] Both the predicted minimum area ratio for which oscillations are sustained as represented by the zero crossings of the plots and the effect of mean pressure follow the same trends seen experimentally. The experiments corresponding to the conditions simulated in Fig. 9 were described by some observers as representing "triggered" instability[5] on the basis that pulsing caused oscillations that did not decay immediately but tended to persist for many cycles of oscillations. The latter behavior is clearly not descriptive of motion near a triggering point; it more accurately describes the approach to the limit cycle. The analysis makes it clear that the experiments correspond to conditions near the lowest limit cycle amplitude. The system is triggered only in the sense that there is a trivial trigger point at zero amplitude; the existence of the rather low limit cycle amplitudes ($\epsilon \sim 0.2$) is indicative of a system which is moderately unstable from the linear standpoint.

Figures 10 and 11 illustrate the sensitivity of the system behavior to motor mean pressure in more detail; the triggering range is encompassed. Curves are shown for a range of burning surface to chamber cross-section area ratios ($S_b/S_c$) similar to those used in the Micheli/Lovine[5] experiments. In Fig. 10, the area ratio is changed by varying the chamber diameter for a set grain sample length. A split grain configuration was assumed with two tubular propellant samples 0.24 m long located at the extreme ends of the chamber as shown in Fig. 1. In Fig. 11, the area ratio is varied for a fixed chamber size (diameter = 1.5 in.) by changing the grain sample length. The trends are very similar, as indicated in a large volume of experimental data; the area ratio is a primary variable for controlling system behavior. The small differences in the plots result mainly from the influence of the nozzle area ratio differences in the two cases.

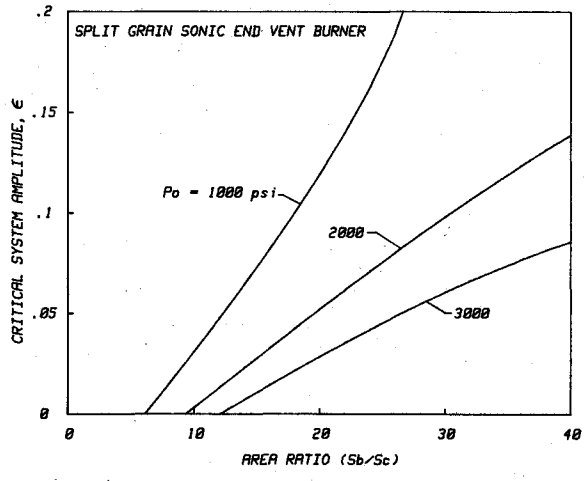


**Fig. 9 Limiting amplitude vs area ratio for simulated sonic end-vent burner.**

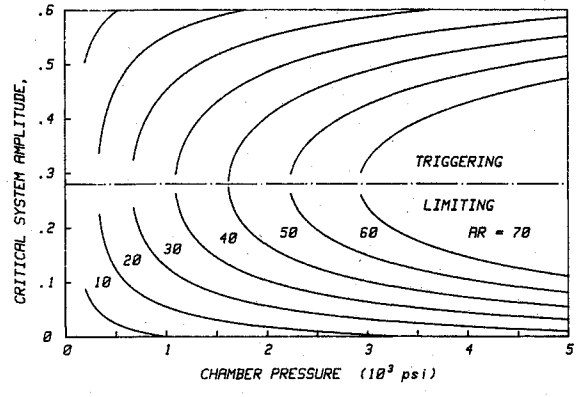


**Fig. 10 Effect of chamber pressure on critical system amplitudes for fixed grain length and variable diameter.**

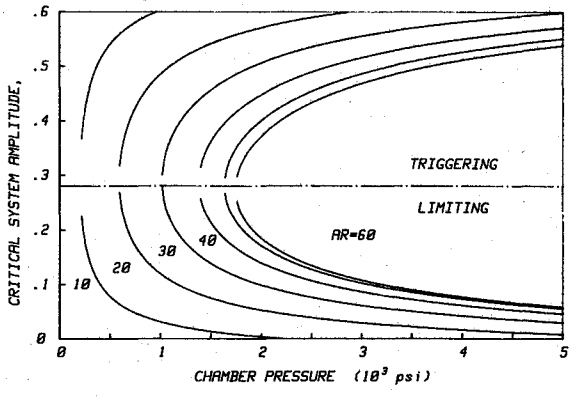


**Fig. 11 Effect of chamber pressure on critical system amplitudes for fixed diameter and variable grain sample length.**

Effects of pulsing on system operation in light of the analytical results is of considerable interest. Figure 12 shows a typical pressure vs time trace for another burner configuration used in the study of Ref. 5. This represents a typical pulser test utilizing a full-length (24 in.) tubular grain. The first pulse at about 0.45 s is damped; the system is linearly stable at the corresponding pressure/nozzle area/burning surface area combination. The pulse at 0.7 s occurs at a point where the threshold of positive $A$ has been crossed; a moderate pulse amplitude of about $\epsilon_{pulse} = 0.15$ causes rapid divergence to a limit cycle with a peak amplitude of approximately 0.3. Several features of the motion are noteworthy;

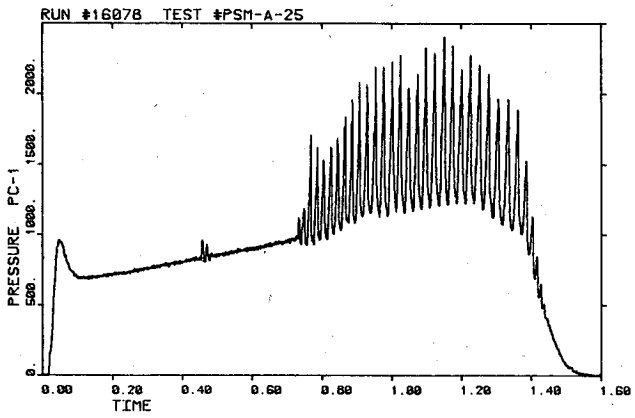


**Fig. 12 Nonlinear combustion response to second pulse in tubular sonic end-vent burner test.**

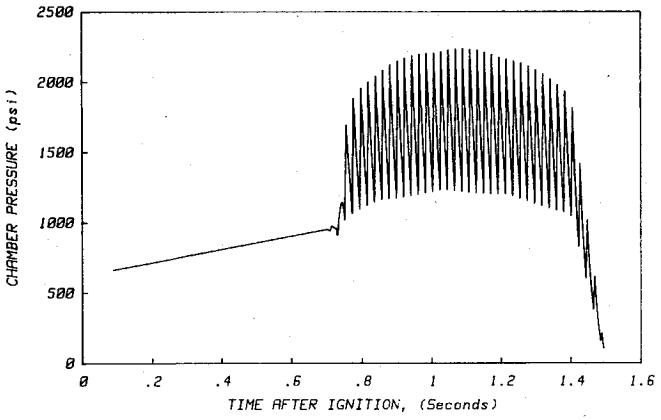


**Fig. 13 Simulated pressure trace for pulsed sonic end-vent burner.**

in particular, another typical attribute of nonlinear oscillatory behavior is exhibited. This is the classical mean pressure shift effect which is still a poorly understood phenomenon. Part of the effect of the pulse is to raise the system mean pressure. This momentarily increases the burning rate above the steady-state value as a result of the increased chamber mean pressure; the mass introduced in the pulse is not instantaneously discharged. Since the rate of growth of global amplitudes, as represented by Eq. (33), depends nonlinearly on the system composite amplitude relative to the chamber mean pressure, the increases in the latter accompanying the growth of the oscillations may significantly enhance the growth rate and the amplitude as measured in physical units. Figure 13 is a simulated firing of this motor, using the third-order analytical model to compute the system amplitude vs time. Since the model does not encompass the mean pressure shift phenomenon explicitly, the experimental mean shift was superimposed. The resulting solution closely resembles the actual data shown in Fig. 12, giving further evidence of the usefulness of the analytical model described here. The frequency exhibited is not the actual frequency of oscillation. In the motor test, time resolution of the low frequency pressure transducer does not allow the high frequency signal to be reproduced correctly; only some of the peaks appear. In the simulation of these results, it was found that similar plots could be produced by varying the plotting time resolution which introduces similar filtering of the output.

## Conclusions

The third-order analysis of combustion instability given here is based on two very strong assumptions: 1) a frozen waveform represented by a superposition of standing waves describing a single traveling shock front and 2) a third-order system energy balance algorithm. Additionally, velocity coupling effects were not incorporated artificially; effects resembling velocity coupling appear in a natural way in the second- and third-order stability integrals. This is not to say that nonlinear combustion response might not play an important role. Evaluations of the terms in the analysis involving nonlinear corrections to the linear pressure coupling have not yet been carried out since neither nonlinear response function data nor a third-order combustion theory is yet available. Progress has been made toward the necessary nonlinear combustion zone analysis,[5] but much remains to be accomplished.

The computational algorithm resulting from the implementation of the analytical findings allows determination of the changes in global system amplitude with time. Major attributes of nonlinear behavior appear naturally. Limit cycle and triggering behavior are inherent characteristics. Extensive computational experience with the resulting model has demonstrated a significant degree of compatibility with experimental data. The utility of the model, both as a tool for use in data analysis and as a framework on which to build improved theoretical understanding of the underlying mechanisms of nonlinear oscillatory combustion, has been demonstrated.

## Acknowledgments

The author wishes to acknowledge the support of this work by the U.S. Air Force Rocket Propulsion Laboratory, Edwards AFB, Calif., under Contract FO4611-81-C-0007 (J. Levine, Contract Monitor) to Aerojet Tactical Systems, Sacramento, Calif. Thanks are due M. J. Ditore, P. L. Micheli, and R. L. Lovine of Aerojet Tactical Systems and F. E. C. Culick of the California Institute of Technology for the benefit of numerous discussions.

## References

[1]Culick, F. E. C., "Nonlinear Behavior of Acoustic Waves in Combustion Chambers," California Institute of Technology, Pasadena, April 1975.

[2]Levine, J. N. and Baum, J. D., "A Numerical Study of Nonlinear Instability Phenomena in Solid Propellant Rocket Motors," *AIAA Journal*, Vol. 21, April 1983, pp. 557-564.

[3]Levine, J. N., Baum, J. D., and Lovine, R. L., "Pulse Triggered Instability in Solid Propellant Rocket Motors," *AIAA Journal*, Vol. 22, Oct. 1984, pp. 1413-1419.

[4]Levine, J. N., Baum, J. D., and Lovine, R. L., "Pulsing of Solid Propellant Rocket Motors: A Numerical and Experimental Study," *Journal of Spacecraft and Rockets*, Vol. 20, March-April 1983, pp. 150-157.

[5]Micheli, P., Lovine, R. L., Flandro, G. A., and Ditore, M., "Nonlinear Stability of Tactical Rocket Motors," Final Report, AFRPL, Edwards AFB, Calif., in review Feb. 1985.

[6]Cantrell, R. H. and Hart, R. W., "Interaction between Sound and Flow in Acoustic Cavities: Mass, Momentum, and Energy Considerations," *Journal of the Acoustical Society of America*, Vol. 36, 1964, pp. 697-706.

[7]Morfey, C. L., "Energy-Balance Equations in Acoustics," *Unstable Combustion of Advanced Solid Propellants*, Bolt, Beranek, and Newmann, Inc., Rept. 1547, Sept. 1967, pp. 6-36.

[8]Andreev, N. N., "Concerning Certain Second-Order Quantities in Acoustics," *Soviet Physics—Acoustics*, Vol. 1, No. 2, 1955, p. 2.

[9]Markham, J. J., "Second-Order Acoustic Fields: Energy Relations," *Physical Review*, Vol. 86, 1952, p. 712.

[10]Markham, J. J., "Second-Order Acoustic Fields: Relations between Energy and Intensity," *Physical Review*, Vol. 89, 1953, p. 972.

[11]Blokhintsev, D. I., "Acoustics of a Nonhomogeneous Moving Medium," NACA TM 1399, 1956.

[12]Schoch, A., "Remarks on the Concept of Acoustic Energy," *Acoustica*, Vol. 3, 1953, p. 181.

[13]Culick, F. E. C., "Flow Effects in Solid Rocket Combustion Instability," Naval Weapons Center, TP 5349, June 1972.

[14]Chu, B. T. and Ying, S. J., "Thermally Driven Nonlinear Oscillations in a Pipe with Traveling Shock Waves," *Physics of Fluids*, Vol. 6, No. 7, Nov. 1963, pp. 1625-1637.

[15]Chester, W., "Resonant Oscillaitons in Closed Tubes," *Journal of Fluid Mechanics*, Vol. 18, 1964, p. 44.

[16]Betchov, R., "Nonlinear Oscillations in a Column of Gas," *Physics of Fluids*, Vol. 1, No. 3, May 1958, pp. 205-212.

[17]Sirignano, W. A. and Crocco, L., "A Shock Wave Model of Unstable Rocket Combustors," *AIAA Journal*, Vol. 2, July 1964, pp. 1285-1296.

[18]Sirignano, W. A., "A Theoretical Study of Nonlinear Combustion Instability: Longitudinal Mode," Dept. of Aerospace and Mathematical Sciences, Princeton University, Princeton, N.J., TR 677, 1964.

[19]Mitchell, C. E., Crocco, L., and Sirignano, W. A., "Nonlinear Longitudial Instability in Rocket Motors with Concentrated Combustion," *Combustion Science and Technology*, Vol. 1, 1969, pp. 35-63.

[20]Rudnick, I., "On the Attenuation of Repeated Sawtooth Shock Wave," *Journal of the Acoustical Society of America*, Vol. 25, 1953, pp. 1012-1013.

[21]Temkin, S., "Nonlinear Gas Oscillations in a Resonant Tube," Bolt, Beranek, and Newmann, Inc., Rept. 1547, Sept. 1967, p. 40.